Measurements of shock-propagation velocities in liquid lead across the metal-nonmetal transition range

A. M. Kondratyev and A. D. Rakhel*

Joint Institute for High Temperatures of Russian Academy of Sciences, Izhorskaya 13, Building 2, Moscow 125412, Russia

(Received 21 February 2023; revised 8 May 2023; accepted 9 May 2023; published 18 May 2023)

The propagation velocities of shock waves with Mach numbers in the range 1.1–1.5 have been directly measured in liquid lead over a wide region of fluid states in the specific volume and pressure plane across the metal-nonmetal transition range. The measured values are compared with those obtained from a caloric equation of state (EOS) constructed using the results of dynamic experiments. The comparison shows that the measured values are in good agreement within the values calculated by the EOS. These results suggest that, for the entire region of the fluid states investigated here (where the fluid is a one-phase system) the shock waves are stable. The values of the critical pressure, critical volume, and critical enthalpy were determined using the EOS and compared with literature data. Thus, the EOS of liquid lead is presented, describing its thermodynamic properties with known accuracy in wide ranges of specific volume and pressure.

DOI: 10.1103/PhysRevB.107.195134

I. INTRODUCTION

Experimental studies of liquid metals in wide ranges of specific volume and pressure are crucial for the development of the theory of condensed states [1–3], theoretical models of astrophysical objects like giant planets and brown dwarfs [4] as well as for nuclear energy applications [5]. When the specific volume of a liquid metal increases, say at a constant pressure, it undergoes two transitions, namely, the liquid-gas phase transition, and the metal-nonmetal transition. On the nonmetallic side of the transition in a plane of specific volume and pressure, the fluid is a dense plasma whose ionization state changes appreciably as the specific volume or pressure is varied [6–8]. Such a partially ionized plasma is characterized by strong coupling between charged particles (i.e., between the conduction electrons and ions) and a partial degeneracy of the electrons [4,9]. The physical theories of such a metal-nonmetal transition and properties of the fluid on the metallic and nonmetallic side of the transition are very uncertain, and experimental data can be used to test the fundamental theories.

Remarkable progress in our understanding of the phenomena in liquid metals is being made owing to the rapid development of high-performance computing. However, despite the significant efforts made, the question of the mechanism of the metal-nonmetal transition occurring in liquid metals and the interrelation between the metal-nonmetal and liquid-gas transitions remains open [10–12]. Recently, to estimate the critical points for the liquid-gas transition in refractory metals, *ab initio* molecular dynamics simulations were used [13,14]. The pressure values on isotherms at several density values were determined for a wide region in the density and pressure plane. The data points on the isotherms were interpolated by third-order polynomials by analogy with the van der Waals equation of state (EOS). Leaving aside the question of the accuracy in the determined values of pressure near the equilibrium line of the phase transition, the question arises of the correct form of the isotherms in the vicinity of the critical point of the liquid metal that undergoes a metal-nonmetal transition. This question is closely related to the question of the correct form of the EOS for this region of the phase diagram.

The EOSs of liquid metals were constructed by using the results of the *ab initio* molecular dynamics simulations [15–17]. In such an EOS, the Helmholtz free energy is represented as a sum of the cold and thermal components, and the latter is divided into the sum of the contributions from the thermal motion of nuclei (ions) and the conduction electrons. The correct analytical forms of the dependencies of the components on the specific volume and temperature are unknown and were obtained by constructing interpolation formulae between the liquid and ideal gas states [18–20]. Such an EOS contains dozens of parameters, which are determined by fitting the dependencies to experimental data or the molecular dynamics simulations results. This approach has two significant difficulties: The analytical form of the EOS in the region of the phase diagram where the liquid-gas and metal-nonmetal transitions occur has not been substantiated, and the errors in the *ab initio* simulations results are not well known. In this paper, we validate the EOS of liquid lead constructed by using an approach which does not have the above difficulties.

To study experimentally the thermophysical properties of liquid metals in wide ranges of specific volume and pressure, the dynamic experimental method [21] was developed which, after several improvements [12,22], made it possible to carry out the measurements with accuracy comparable with that of the static experiments [6,23]. Recently, this method was used to measure the thermodynamic functions and electrical resistivity of liquid lead [22] and lead-bismuth eutectic [12] over wide regions of fluid states in the VP plane (V is the

*rakhel@oivtran.ru

specific volume, and P is pressure). Based on the experimental data and by using the phenomenological approach [24], the caloric EOSs have been constructed for these two metals, which allow the critical points for the liquid-gas transitions and the critical density for the metal-nonmetal transitions to be determined [12]. As shown in Ref. [24], the error in such a caloric EOS depends only on the errors in the experimental data used to determine the characteristic functions of the EOS, which are directly derived from the measured quantities, and therefore, the error in the EOS can be estimated. However, for a wide region of the VP plane in which experimental data have been obtained by the dynamic technique, corresponding to the ranges of the relative volume $V/V_0 = 1.3$–8 (V_0 is the normal value of the specific volume), and the pressure $P = 0.5$–5 GPa, there are no other experimental data. The literature data for liquid lead are only available in the ranges $P \leqslant 0.3$ GPa, $V/V_0 < 2$. Hence, for a wide region of the VP plane, the experimental data [12,22] cannot be compared with data obtained by a different experimental technique. This situation does not allow a reliable estimate of the possible systematic errors in the dynamic measurements to be made. Since the results obtained in Refs. [12,22] and the conclusions drawn from them are of considerable interest, the problem of estimating the systematic errors in the pulse experiments is of particular importance.

The van der Waals EOS is a particular case of the Mie-Grüneisen EOS [24]. As was already mentioned, the present EOS allows the critical density for both the liquid-gas and metal-nonmetal transitions to be determined. For other liquid metals, the critical density for the metal-nonmetal transition has not yet been obtained, neither from the quantum molecular dynamics simulations results nor from the results of the static experiments [6,11,12]. The van der Waals EOS makes no difference between a metal and a nonmetal. The fact that the van der Waals EOS may not be quite correct in this region follows from the behavior of the sound velocity predicted by the present EOS which indicates that, at the critical point, the velocity of sound tends to zero. Such behavior does not generally follow from the van der Waals EOS [25].

In this paper, a time-of-flight method has been developed for direct measurements of the propagation velocities of weak shock waves generated in the samples of the dynamic experiments. Such shock waves cause relatively small jumps in density of the samples, but their velocity may noticeably exceed the velocity of sound in the state in front of the shock wave. The Mach numbers for these shocks, i.e., the ratio of the shock velocity to the velocity of sound in the initial state, are within the range 1.1–1.5. Since the Hugoniot curves for liquid lead can be determined from the caloric EOS whose precision depends only on the precision of the experimental data used to determine the characteristic functions [24], the comparison of the measured values of the shock wave velocity with those obtained from the EOS allows the systematic errors of the dynamic experiments to be estimated. The accuracy of the EOS depends only on the accuracy of the experimental data since no simplifying assumptions were made when deriving the analytical form of the EOS. The time-of-flight methods are frequently applied to measure the velocities of shock and sound waves in dynamic experiments by using a laser pulse to create a pressure perturbation and measuring the transit time of the perturbation in the material under study. In Ref. [26], the velocity interferometer for any reflector was used to measure the transit times of sound waves in silicon compressed by shock waves up to pressures of 2 TPa.

It should be noted that experimental data on the shock-propagation velocity for the fluid states across the metal-nonmetal transition range are also of considerable interest in connection with the theoretical predictions of the mechanical instability of the electron Fermi liquid in this range [27–29] and the question of the influence of quantum fluctuations on thermodynamic functions [2,30]. In this paper, we report on the measurement results on the shock-propagation velocity obtained for the entire region of fluid states in the VP plane studied earlier [22]. Comparison of the measured shock-propagation velocities with those determined from the caloric EOS has shown reasonably good agreement. Based on the comparison, an accurate estimate of the systematic errors in the dynamic experiments was made, and thus, the accuracy of the EOS was tested.

II. METHOD FOR MEASURING THE PROPAGATION VELOCITY OF WEAK SHOCK WAVES IN THE DYNAMIC EXPERIMENTS

The submicrosecond pulse-heating technique [21,22] used here, designed to study the thermophysical properties of expanded liquid metals, is as follows. A metal sample in the form of a square piece of foil is sandwiched between two transparent plates of the so-called window material (silica glass or sapphire plates in these experiments) and resistively heated by an electric current pulse with an amplitude of 10–100 kA and a rise time $\sim$1 μs from a capacitor discharge system. In the experiment, the electric current in the sample, the voltage across it, and the displacement of the sample surface caused by the thermal expansion are measured. This set of measured quantities allows the temporal dependences of the specific internal energy, specific volume, pressure, and resistivity for each experiment to be determined. The duration of these experiments in the case in which the sapphire plates are used does not exceed 1 μs, and for the experiments with the silica glass plates, it is $<$2 μs. These conditions determine the interval of time during which the sample remains homogeneous, and the thermal expansion is one dimensional.

In addition to the measured quantities listed above, in this work, we measure the velocity of weak shock waves in such dynamic experiments. The essence of the method used here to perform these measurements is as follows. In the dynamic experiment, i.e., during the ohmic heating of the sample by an electric current pulse, at a predetermined instant t_1 when the sample is in the state of interest for which the shock wave velocity is to be measured, one of the sample surfaces (which we call here the front surface) is irradiated by a short laser pulse. The time t_1 is determined from the previously measured (in a similar experiment) temporal dependences of the specific volume and pressure in the sample. The laser pulse used in this experiment had sufficient energy to create a well-defined pressure perturbation (a weak shock wave) on the front surface of the sample, and that remained so on the opposite surface (back surface), where it arrived with some delay. By measuring the instant of generation of the perturbation at the front surface

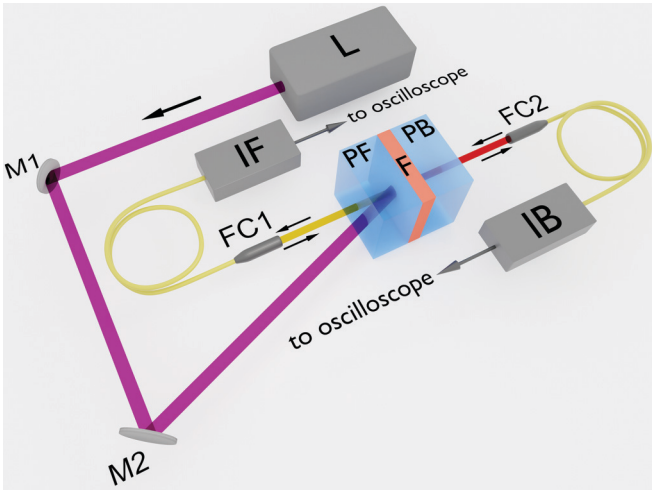

FIG. 1. Schematic layout for the measurements of the shock-propagation velocity in the dynamic experiments. F is the sample (a piece of foil), PF and PB are the front and back plates of the window material, L is a pulsed laser, IF and IB are the front and back interferometers, M1 and M2 are dielectric mirrors, and FC1 and FC2 are fiber collimators.

and the instant of its arrival at the back surface of the sample and knowing the change in the thickness of the sample with time (which is measured in the experiment), we determine the velocity of the perturbation. A scheme of such measurements is shown in Fig. 1.

To produce the pressure perturbations, a New Wave Research pulsed laser (Orion model) was used, which generates a laser pulse at the wavelength of 1064 nm, having a duration of ∼7 ns and an energy of ∼29 mJ. Due to the attenuation of the laser pulse along the optical path, the laser pulse incident on the sample front surface had an energy of ∼22 mJ. The laser beam was focused on the front surface of the sample to a spot with a diameter of 1 mm. The collimated beam of the fiber laser interferometer IF (see Fig. 1) was reflected from the same area. The reflecting spot diameter on the sample surface (or more precisely, the beam was reflected from a dielectric mirror deposited on the surface of the window in contact with the sample) was ∼0.3 mm. A more detailed description of the interferometer can be found elsewhere [12,22].

It is well known that, in a conductor, the laser pulse energy penetrates only to a relatively small depth δ, determined by the formula:

$$\delta = \frac{\mathrm{c}}{\sqrt{2\pi\omega\sigma}}, \tag{1}$$

(the normal skin effect [31]), where c is the velocity of light in vacuum, ω is angular frequency of the laser light, and σ is the electrical conductivity of the sample. In the metallic state, the resistivity of liquid lead (i.e., the reciprocal of the conductivity) is in the range $\sigma^{-1} =$ 2–10 μΩ m [22], so that we obtain from Eq. (1) $\delta = 0.05-0.1$ μm. Absorption of the laser pulse energy in the layer of the thickness $\sim\delta$ leads to intense heating of the layer. As a result, a traveling pressure perturbation arises in the sample. A typical thickness of the samples in the measurements of the velocity of the shock waves was $h =$ 30–100 μm, that is much larger than δ, but

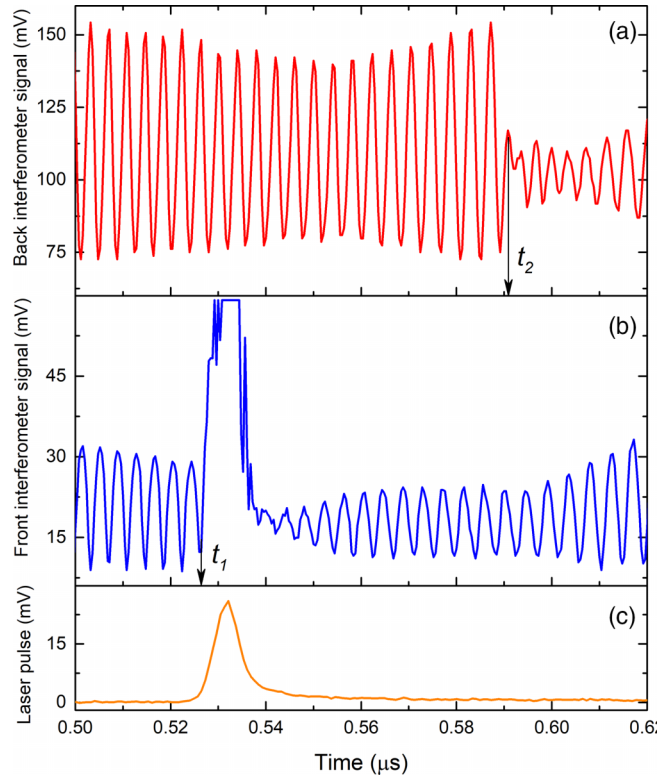

FIG. 2. (a) Oscillogram of the interferometer IB from which the instant t_2 is determined. (b) Oscillogram of the interferometer IF used for detection of the instant t_1. (c) Temporal dependence of the radiation intensity produced by the pulsed laser.

is much less than the diameter of the spot irradiated by the laser pulse. Thus, the pressure perturbations are rather short compared with the duration of the dynamic experiments and nearly one dimensional.

The time of appearance of the perturbation at the front surface of the sample t_1 is detected by the interferometer IF (see Fig. 1). To increase the accuracy of the measurement, a dielectric mirror is deposited on the side of the plate PF in contact with the sample. The moment of arrival of the perturbation to the back surface of the sample t_2 is detected by another interferometer (the interferometer IB in Fig. 1). A dielectric mirror is also deposited on the surface of the plate PB in contact with the sample. The interferometer IB is identical to the interferometer IF and uses the same laser source. The velocity of propagation of the pressure perturbations in the sample is determined by the formula:

$$D = \frac{h_1 + h_2}{2(t_2 - t_1)}, \tag{2}$$

where h_1 and h_2 are the thickness of the sample at instants t_1 and t_2, respectively. A derivation of this formula is given in Sec. III.

The oscillograms of the two displacement interferometers for a typical experiment in this paper illustrating accuracy of the detection of the instants t_1 and t_2 are shown in Fig. 2. The oscillograms were recorded by a Rohde&Schwarz RTM2104 oscilloscope using Thorlabs DET01FC photodetectors. The abrupt increase in the amplitude of the front interferometer

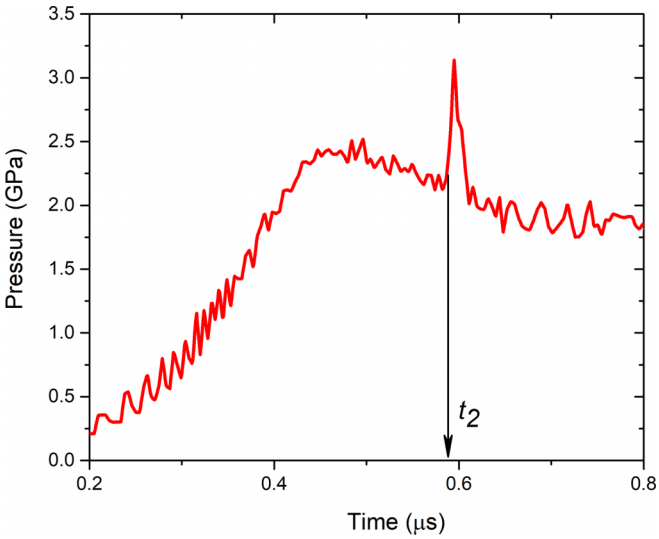

FIG. 3. Temporal dependence of the pressure at the back surface of the sample, obtained from the oscillogram shown in Fig. 2(a). t_2 is the instant when the pressure perturbation reaches the back surface of the sample.

signal after the time t_1 is caused by illumination of this interferometer by the radiation of the pulsed laser. As seen from Fig. 2(a), the repetition rate of the extrema in the oscillogram of the back interferometer increases remarkably after the arrival of the perturbation, which indicates an increase in the velocity of this surface.

The origin $t = 0$ in Fig. 2 corresponds to the time when the electric current starts to flow through the sample. The temporal dependence of the radiation intensity emitted by the pulsed laser that is used to generate the pressure perturbation in the sample is shown in Fig. 2(c). This signal was obtained by reflecting the laser pulse from one of the dielectric mirrors used in the optical scheme (see Fig. 1). The energy of this pulse is $<1\%$ of that of the incident laser pulse. As seen from the Fig. 2, the illumination of the front interferometer by the pulsed laser allows us to prove that the synchronization of these optical measurements was performed with an accuracy of not worse than 1 ns. Figure 3 gives the temporal dependence of the pressure at the back surface of the sample, obtained from the oscillogram represented in Fig. 2(a). The method used here to determine the pressure is presented elsewhere [22]. It should be mentioned that, in the experiment from which the oscillograms are shown in Fig. 2, the windows were of silica glass. As seen from the Fig. 3, at the instant t_2, the pressure at the back surface of the sample begins to rise abruptly, which indicates the arrival of the shock wave. Thus, the temporal dependence of the back surface displacement of the sample measured in this experiment makes it possible to determine both the pressure in the sample before the arrival of the perturbation and the pressure jump created by it.

The foils from which the samples were cut for these experiments were made by rolling ingots of lead (lead of grade C0000 with a Pb content of at least 99.9999 wt. %) on YuMO-V9 jewelry rollers. The foils used in these experiments had the thickness of 10–50 μm.

To estimate some errors in the measurements of the velocities of the pressure perturbations in the lead samples, we performed the measurements for the sample under normal conditions. In this case, the same experimental assemblies were taken, consisting of two sapphire plates and the lead foil strip sandwiched between them, which were used in dynamic experiments, but the pressure perturbation was produced in the sample under normal conditions (there was no electric current pulse through the sample). As a result of the present measurements made in 13 experiments, we obtained the average value of the velocities of 2.18 ± 0.09 km/s. In these experiments, the errors in determining the pressure in the waves are relatively large since the layers of glue between the sample and the sapphire plates are not yet compressed by the sample, and this compression occurs only in the perturbation waves. This error is greater, the lower the pressure is in the wave. However, the measurements have shown that the pressures in the waves exceeded the Hugoniot elastic limit for lead ($P_{\mathrm{HEL}} < 0.4$ GPa [32]). Therefore, it is reasonable to compare the measured values of the velocities of the waves here not with the longitudinal sound velocity of lead but with the shock wave velocity on the Hugoniot curve. We made such a comparison using the dependence of the shock wave velocity on the particle velocity from Ref. [33]. The comparison showed that, to within the error in the measurements of the velocity jumps in the waves, our results agree with the values of the shock waves velocities. For the waves with the pressure of 4 GPa, we measured the velocity of 2.27 km/s, which is in fair agreement with the shock wave velocity on the Hugoniot curve of 2.22 km/s [33]. For waves with lower pressures, the agreement is worse.

III. MEASUREMENT RESULTS

The measurement results obtained in the present experiments on the velocity of weak shock waves in liquid lead are shown in Fig. 4. The measured velocity values are represented as a function of the relative density V_0/V, i.e., the ratio of the density $\rho = V^{-1}$ to its normal value $\rho_0 = 11.34$ g/cm^3. Near each measured value of the velocity, the pressure in the sample in front of the perturbation (i.e., a weak shock wave) and the pressure behind the shock wave are indicated (in GPa). Note that a shock wave can be considered weak if it causes a jump in the specific volume which is much smaller than the specific volume in front of the shock wave. In the present experiments, the ratio of the jump in the specific volume to the value of the volume in the initial state (in front of the shock wave) did not exceed 0.3, and for most of the experiments, it was <0.2. The blue crosses in Fig. 4 indicate three experiments for which the Hugoniot curves are shown in Fig. 5. The curves start from the initial states for which the measurements of the shock-propagation velocity were made. The data points represent the results of measurements for three significantly different states of the fluid, namely, the metallic state, the state with a density close to the critical density for the liquid-gas transition, and the plasma state (i.e., a gaseous nonmetallic state) [12,22]. As follows from Fig. 4, in the range $V_0/V > 0.6$, where the velocity of sound in liquid lead is relatively high, the measured values of the velocity of weak shock waves here at pressures of 1.0–1.5 GPa practically coincide with the values of the

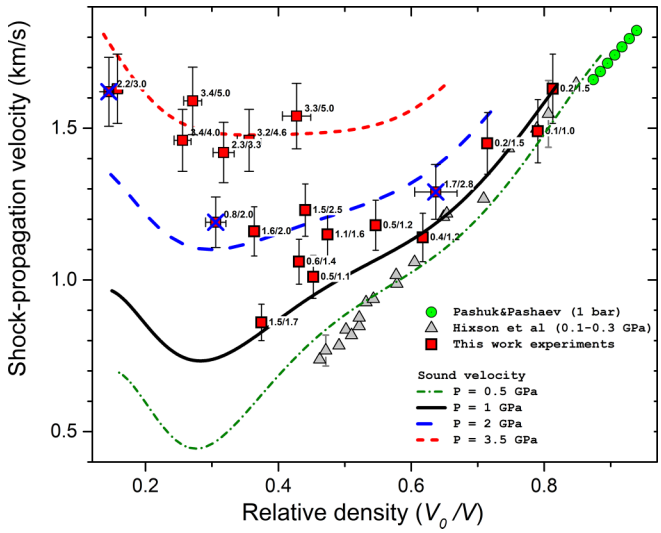

FIG. 4. Velocity of weak shock waves as a function of the relative density (V_0 is the specific volume of lead under normal conditions): red squares are the values measured in this paper. The two numbers next to the squares are the pressure values in the sample in front of the shock wave and behind it, respectively (in GPa). Blue crosses mark experiments for which the Hugoniot curves are given in Fig. 5. The lines represent the dependencies of the velocity of sound in lead on the density in the liquid and gaseous state along isobars $P = 0.5, 1, 2$, and 3.5 GPa obtained from the caloric equation of state (EOS). The green circles and the gray triangles are the sound velocity values measured in the static experiments [34] and the dynamic experiments [35], respectively.

velocity of sound measured in the range of 0.1–0.3 GPa [35]. At the lower densities, $V_0/V < 0.6$, the shock wave velocity values we obtained noticeably differ from the values of the velocity of sound in Ref. [35]. Due to methodological difficulties, we failed to perform the measurements for the shock waves which are so weak that their velocities in this density range are close to the sound velocity values at pressures of 0.1–0.3 GPa. In these dynamic experiments, we were not always able to detect the pressure perturbations which caused pressure jumps <0.5 GPa. For such perturbations, the features in the oscillograms shown in Fig. 2 (the kinks) were not well pronounced, so that their detection was difficult. To demonstrate the dependence of the sound velocity on the relative density and pressure, the isobars $P = 0.5$, 1, 2, and 3.5 GPa obtained from the caloric EOS are presented in Fig. 4. These isobars show the expected dependencies for the shock-propagation velocity in the case in which the pressure jumps in the shocks are infinitesimal.

The errors in the measured values of the shock wave velocity and the relative density are shown in Fig. 4. We estimate the maximum error in the density values as <4%. The major contribution to the experimental error in the shock wave velocity gives the errors in the quantities which enter the formula in Eq. (2). We proceed now to derive this formula.

In these experiments, we detect the instant of generation of the shock wave on the front surface of the sample t_1 and the instant of arrival of this wave on the back surface t_2. Since the window plates in the experimental assembly have equal dimensions, the assembly has a symmetry plane that passes through the center of mass of the sample and is parallel to the front and back surface. Let us take the origin of the system of coordinates at the center of mass of the sample, with the x axis being perpendicular to the surfaces in the direction from the front surface to the back. In this system of coordinates, the velocity of a pressure perturbation is $D + u$, where D is the velocity of the perturbation relative to the fluid, and u is the local velocity of the fluid (we assume that the velocities have x components only). It is obvious that the time required for the perturbation to traverse the distance from the front to the back surface is related to the instantaneous positions of

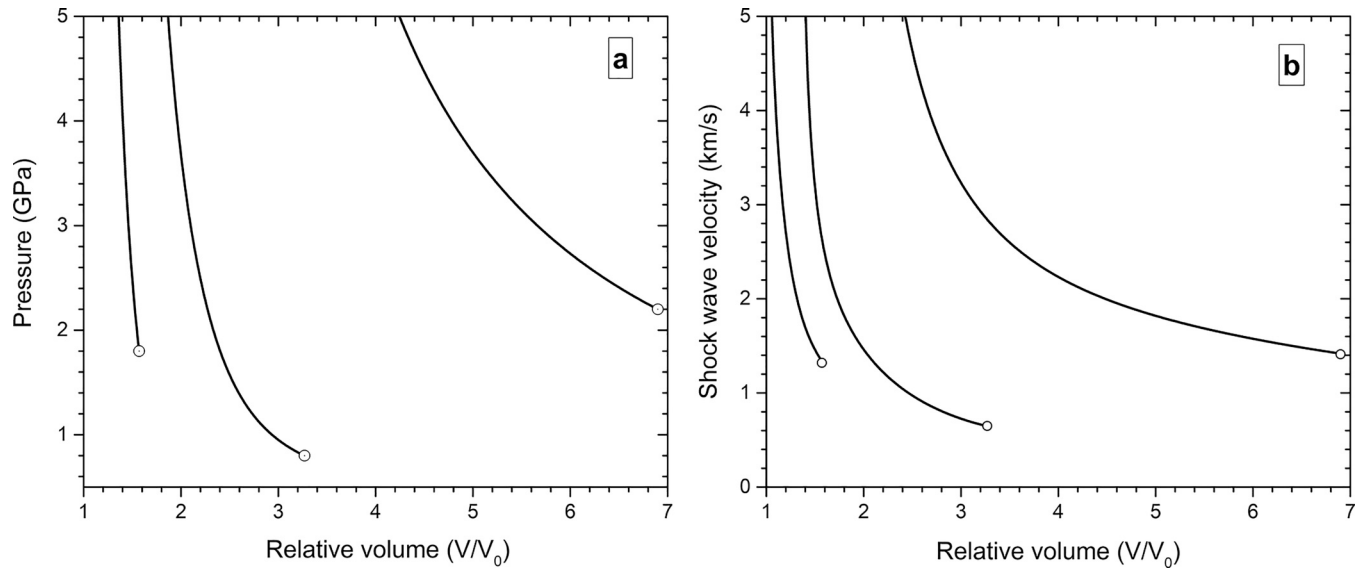

FIG. 5. (a) Hugoniot curves for liquid lead calculated from the caloric equation of state (EOS) in the plane of the relative volume and pressure for three experiments, indicated with blue crosses in Fig. 4. The circles are the initial states on the Hugoniot curves. (b) The same Hugoniot curves in the relative volume and shock-propagation velocity plane.

these surfaces at the instants t_1 and t_2 by

$$\int_{t_1}^{t_2} [D(x,t) + u(x,t)]dt = 0.5[h_2 + h_1], \quad (3)$$

where h_1 and h_2 are the thicknesses of the sample at instants t_1 and t_2, respectively. In view of the symmetry of the experimental assembly, the relative smallness of the velocity of the fluid, and the variation in the velocity of the perturbation during the interval t_2-t_1, the integral of $u(x,t)$ on the left side of the relation in Eq. (3) can be neglected, and we obtain the formula in Eq. (2) in which D is the averaged velocity over the time t_2-t_1.

Now let us return to the estimation of the error in the velocity D by the formula in Eq. (2). The difference $t_2 - t_1$ was determined from the oscillograms with an accuracy of 2 ns, and synchronization of the two interferometers was made with an accuracy of not worse than 0.3 ns. This contributes 2–7% to the relative error in the difference $t_2 - t_1$, depending on the experimental conditions. The relative error in determining the thicknesses h_1 and h_2 was ∼4%, and for the thinnest foils, it reached 5%. Summing up the listed relative errors (as the square root of the sum of squares of the contributions), we obtain the errors in the shock wave velocity values in the range 5–9%, which are shown in Fig. 4. The error in the measured values of pressure in front of the shock waves (which are indicated in Fig. 4) did not exceed 6%, and the error in the pressure values behind the shock waves was no worse than 20%.

IV. INTERPRETATION AND DISCUSSION OF THE RESULTS

Figure 4 shows that the present results are only in qualitative agreement with the calculations of the velocity of sound by the caloric EOS. If we compare the measured value of the velocity of the perturbation with the corresponding sound velocity (on the nearest isobar), it becomes clear that these quantities are closer when the pressure in the sample is closer to the pressure on this isobar and when the pressure jump caused by the perturbation is smaller. To make a quantitative comparison for the shock waves with larger jumps, let us compare their velocities with the velocity of shock waves calculated by the EOS. As was shown in Sec. II, in these experiments, we measure not only the pressure at the back surface of the sample before the arrival of the perturbation but also the pressure jump caused by it. Figure 5 shows three Hugoniot curves for liquid lead calculated from the present EOS. The initial states on these curves are the states for which the shock wave velocities were measured, and these states are indicated with the blue crosses in Fig. 4.

As shown in Ref. [22], the caloric EOS of liquid lead has the form of the Mie-Grüneisen EOS:

$$P = P_c(V) + \frac{\gamma(V)}{V}[E - E_c(V)], \quad (4)$$

where $E_c(V)$ and $P_c(V)$ are the cold components of the specific internal energy and pressure, respectively, and $\gamma(V)$ is the Grüneisen coefficient, which is a function only of specific volume. The statement that the EOS of liquid lead has the form in Eq. (4) results from the fact that the isochores plotted in the plane of the specific internal energy and pressure are straight lines. This property of the isochores was established and carefully examined in Ref. [22]. From the above fact, using the familiar thermodynamic relations can be rigorously derived, the EOS having the form of the Mie-Grüneisen EOS [24]. In the EOS, the characteristic functions, i.e., the dependencies $\gamma(V)$, $E_c(V)$, and $P_c(V)$, can be determined directly from the experimental data. The accuracy of these dependencies depends only on the accuracy of the data. The dependence $\gamma(V)$ for liquid lead is presented in Ref. [22], and the cold components of energy and pressure were obtained in the same way as for the lead-bismuth eutectic [12] based on the experimental data [22]. The analytical functions approximating the experimental data points for these dependencies are given in the Appendix. The functions have rather arbitrary forms, and the only requirement was to approximate the experimental data within the range of the experimental errors. At present, there are no physical models that can describe these dependencies and hence predict their correct analytical forms.

It can be shown that, for the Mie-Grüneisen EOS in Eq. (4), the Hugoniot curve can be represented in the analytical form:

$$P = \frac{VP_c(V) + \gamma(V)[E_1 - E_c(V) - 0.5P_1(V_1 - V)]}{V - 0.5\gamma(V)(V_1 - V)}, \quad (5)$$

where P and V are the values of pressure and specific volume on the Hugoniot curve, and index 1 denotes the values of the quantities in the initial state (i.e., in the state in front of a shock wave).

The sound velocity, which we denote by c_s, can also be represented in the analytical form:

$$c_s = V\left\{-P_c'(V) + \left[\frac{\gamma}{V} - \left(\ln\frac{\gamma}{V}\right)'\right][P - P_c(V)]\right\}^{1/2}, \quad (6)$$

where the prime denotes differentiation with respect to V. Hence, the caloric EOS of liquid lead constructed here made it possible to calculate the Hugoniot curves and the sound velocity values for the entire region of the fluid states in the VP plane investigated here. As seen from Fig. 5, the Hugoniot curves do not have the sections for which the derivative of the pressure with respect to the specific volume is positive and where the shock wave is unstable [36]. We have also checked that the sign of the second derivative of the specific volume with respect to the pressure along isentropes is positive, i.e., the condition

$$\left(\frac{\partial^2 V}{\partial P^2}\right)_S > 0 \quad (7)$$

is fulfilled for the entire region of interest, so that the shock waves are compression waves rather than rarefaction waves [36].

Let us compare the velocities of the pressure perturbations measured here with the corresponding shock wave velocity values calculated by the EOS. We shall consider the middle experiment of the three indicated in Fig. 4 by the blue crosses for which the relative density in the initial state is 0.31. In this case, the pressure in the sample at the instant t_1 was ∼0.8 GPa, and the velocity of sound for this state, according to the EOS, is 0.7 km/s. For this experiment, the measured pressure at the back surface of the sample after the arrival of the perturbation

TABLE I. Values of the shock-propagation velocity inferred from the experiment D_{exp} are compared with the calculated ones D_{calc}. Here, P_1 and P_2 are the pressure values in front of the shock wave and behind it, respectively; V_0/V_1 is the relative density in the initial state; d_0 is the initial thickness of the foil (sample); and $\delta D = |D_{calc} - D_{exp}|/D_{exp}$.

Exp. No.	V_0/V_1	P_1 (GPa)	P_2 (GPa)	$t_2 - t_1$ (ns)	d_0 (mm)	D_{exp} (km/s)	D_{calc} (km/s)	δD (%)
21	0.546	0.5	1.2	46	29.7	1.18	1.11	5.9
24	0.364	1.6	2.0	87	36.6	1.16	1.12	3.4
25	0.474	1.1	1.6	68	37.2	1.15	1.12	2.6
32	0.375	1.5	1.7	118	38.0	0.86	0.98	14.0
35	0.617	0.4	1.2	28	19.8	1.15	1.21	5.2
36	0.813	0.2	1.5	24	31.9	1.63	1.7	4.3
37	0.714	0.2	1.5	30	31.1	1.45	1.41	2.8
41	0.441	1.5	2.5	59	31.9	1.23	1.19	3.3
42	0.791	0.1	1.0	25	29.4	1.49	1.53	2.7
44	0.452	0.5	1.1	65	29.7	1.01	0.99	2.0
53	0.431	0.6	1.4	64	29.3	1.06	1.04	1.9
54	0.256	3.4	4.0	38	14.2	1.46	1.62	11.0
57	0.145	2.2	3.0	65	15.3	1.62	1.65	1.9
58	0.317	2.3	3.3	34	15.3	1.42	1.41	0.7
59	0.306	0.8	2.0	27	9.8	1.19	1.10	7.6
60	0.158	1.8	2.6	35	9.0	1.63	1.49	8.6
64	0.271	3.4	5.0	34	14.7	1.6	1.77	10.6
65	0.356	3.2	4.6	26	13.5	1.46	1.65	13.0
66	0.637	1.7	2.8	17	14.0	1.29	1.5	16.3
67	0.427	3.3	5.0	22	14.5	1.54	1.69	9.7

was 2.0 GPa. As follows from Fig. 5(a), the relative volume behind the shock wave for this pressure is ∼2.3, and according to Fig. 5(b), for this volume, the shock wave velocity is 1.1 km/s. As seen from Fig. 4, the measured value of the velocity of the perturbation is ∼1.2 km/s. Therefore, to within the experimental error of this paper and Ref. [22], where the experimental data used to construct the EOS here had been obtained, these two values are in close agreement.

A similar comparison of the measured shock-propagation velocity with the corresponding value calculated by the caloric EOS has been carried out for all experiments in this paper. The reader can easily make such a comparison for the other two experiments marked in Fig. 4 with the blue crosses, for which the Hugoniot curves are presented in Fig. 5. The comparison for all experiments in this paper is presented in Table I. As seen from this table, the difference between the measured values of the shock-propagation velocity and the calculated ones is <10% for most experiments, except those with relatively thin samples and that with the thickest sample for which the difference $t_2 - t_1$ becomes relatively large and the formula in Eq. (2) becomes not sufficiently accurate.

Thus, the comparison shows that, to within the experimental error, the values of the shock-propagation velocity measured here agree with the values predicted by the caloric EOS. Since the uncertainties in the quantities obtained from the EOS are determined mainly by the errors in the experimental data [22] used to obtain the characteristic functions of the EOS, the present results also provide strong evidence that the systematic errors in the dynamic experiments [12,22] had been estimated correctly.

In the region of the VP plane investigated here, the fluid is a one-phase system. This conclusion was made based on the values of the critical density and critical pressure determined from the caloric EOS. Since now we know with reasonable confidence the accuracy of the EOS, we can determine both the critical density and critical pressure of the fluid using the procedure described in Ref. [12] and estimate the uncertainties in these values. As a result, we found for the critical density the value $\rho_c = 3.2 \pm 0.2$ g cm^{-3} and for the critical pressure $P_c = 0.21 \pm 0.01$ GPa. These values are in excellent agreement with the estimates made in Refs. [18,37–40]. In addition to these quantities, we have determined the critical enthalpy $W_c = 1.02 \pm 0.07$ kJ g^{-1} (more precisely, it is the difference between the critical enthalpy and its value in the normal state). The value of the critical enthalpy obtained here is a bit higher than that estimated in Ref. [39], 0.85 kJ g^{-1}, but lower than that which follows from the data presented in Ref. [37], $W_c \leqslant 1.2$ kJ g^{-1}. The literature estimates of W_c were made based on the observation of the behavior of the electrical resistivity along isobars.

V. CONCLUSIONS

An experimental technique has been developed which allows direct measurements of the shock-propagation velocities to be made over a wide region of fluid states in the density and pressure plane. The measurement results obtained in this paper have been used to obtain an accurate estimate of the systematic error in the exploding foil experiments (<5%) [12,22]. The measurement results are in good agreement with the predictions of the caloric EOS constructed using the data of the dynamic experiments. Based on the present results, it can also be concluded that the one-dimensional shock waves generated by the laser pulses in these experiments were of sufficient stability to enable the measurement of their velocity for the sample thicknesses evaluated.

ACKNOWLEDGMENTS

This paper was funded by Russian Foundation for Basic Research and ROSATOM, Project No. 20-21-00093.

APPENDIX

The fitting function to the experimental data points in Ref. [22] for the dependence of the Grüneisen coefficient on the relative volume:

$$\gamma = A_1 + \frac{A_3 p}{1 + \exp[k_1(y_1 - y)]} + \frac{A_3\,(1-p)}{1 + \exp[k_2(y_2 - y)]}, \tag{A1}$$

where $y = \ln(V/V_0)$, $A_3 = A_2 - A_1$, and the best fit values of the parameters are as follows: $A_1 = 0.32852$, $A_2 = 3.73608$, $y_1 = 0.11388$, $y_2 = 0.75668$, $k_1 = -4.05931$, $k_2 = -1.48531$, and $p = 0.78365$.

The function $b(V)$, which is used to determine the cold components of the internal energy and pressure [24], and defined as

$$b = E_c(V) - \frac{V}{\gamma(V)}\,P_c(V) \tag{A2}$$

was approximated by the polynomial:

$$b = \sum_{n=1}^{n=8} B_n y^n, \tag{A3}$$

where $y = \ln(V/V_0)$, and the best fit values of the parameters are $B_1 = 1.07432$, $B_2 = 1.50417$, $B_3 = -7.81034$, $B_4 = 16.7692$, $B_5 = -19.29587$, $B_6 = 11.70594$, $B_7 = -3.53087$, and $B_8 = 0.41797$.

[1] N. F. Mott, *Metal–Insulator Transitions* (Taylor and Francis, London, 1990).

[2] S. Sachdev, *Quantum Phase Transitions* (Cambridge University Press, Cambridge, 2011).

[3] *Metal-to-Nonmetal Transitions*, edited by R. Redmer, F. Hensel, and B. Holst (Springer, Berlin, 2010).

[4] *Frontiers and Challenges in Warm Dense Matter*, edited by F. Graziani, M. P. Desjarlais, R. Redmer, and S. B. Trickey (Springer, Cham, 2014), Vol. 96.

[5] National Research Council, *Frontiers in High Energy Density Physics: The X-Games of Contemporary Science* (National Academies Press, Washington, DC, 2003).

[6] F. Hensel and W. W. Warren, Jr., *Fluid Metals: The Liquid–Vapor Transition of Metals* (Princeton University Press, Princeton, 1999).

[7] A. L. Khomkin, A. S. Shumikhin, and Rakhel, J. Exp. Theor. Phys. **130**, 602 (2020).

[8] E. M. Apfelbaum, Contrib. Plasma Phys. **61**, e202100063 (2021).

[9] V. Fortov, I. Iakubov, and A. Khrapak, *Physics of Strongly Coupled Plasma* (Oxford University Press, New York, 2006).

[10] L. D. Landau and Ya. B. Zeldovich, Zh. Eksp. Teor. Fiz. **14**, 32 (1944) [Acta Phys.-Chim. USSR **18**, 194 (1943)]. [L. D. Landau, in *Collected Papers of L. D. Landau*, edited by D. Ter Haar (Pergamon, 1965), pp. 380–382].

[11] G. Kresse and J. Hafner, Phys. Rev. B **55**, 7539 (1997).

[12] A. M. Kondratyev, V. N. Korobenko, and A. D. Rakhel, J. Phys.: Condens. Matter **34**, 195601 (2022).

[13] D. V. Minakov, M. A. Paramonov, and P. R. Levashov, Phys. Rev. B **103**, 184204 (2021).

[14] D. V. Minakov, M. A. Paramonov, and P. R. Levashov, Phys. Rev. B **97**, 024205 (2018).

[15] T. Sjostrom, S. Crockett, and S. Rudin, Phys. Rev. B **94**, 144101 (2016).

[16] C. J. Wu, P. C. Myint, J. E. Pask, C. J. Prisbrey, A. A. Correa, P. Suryanarayana, and J. B. Varley, J. Phys. Chem. A **125**, 1610 (2021).

[17] D. A. Rehn, C. W. Greeff, L. Burakovsky, D. G. Sheppard, and S. D. Crockett, Phys. Rev. B **103**, 184102 (2021).

[18] L. V. Al'tshuler, A. V. Bushman, M. V. Zhernokletov, V. N. Zubarev, A. A. Leont'ev, and V. E. Fortov, Sov. Phys. JETP **51**, 373 (1980).

[19] G. I. Kanel, S. V. Razorenov, and V. E. Fortov, *Shock-Wave Phenomena and the Properties of Condensed Matter* (Springer, New York, 2004).

[20] S. P. Lyon and J. D. Johnson, SESAME: The Los Alamos National Laboratory equation of state database, Tech. Rep. LANL LA-UR-92-3407 (Los Alamos National Laboratory, Los Alamos, USA, 1992).

[21] V. N. Korobenko and A. D. Rakhel, Phys. Rev. B **75**, 064208 (2007).

[22] A. M. Kondratyev, V. N. Korobenko, and A. D. Rakhel, J. Exp. Theor. Phys. **127**, 1074 (2018).

[23] K. I. Kikoin and A. P. Senchenkov, Fiz. Metal. Metalloved. **24**, 843 (1967) [Phys. Met. Metall. **24**, 74 (1967)].

[24] A. D. Rakhel, J. Phys.: Condens. Matter **30**, 295602 (2018).

[25] L. D. Landau and E. M. Lifshitz, *Statistical Physics. Part 1 (Course of Theoretical Physics, Vol. 5)*, 3nd ed. (Pergamon Press, Oxford, 1980).

[26] B. J. Henderson, M. C. Marshall, T. R. Boehly, R. Paul, C. A. McCoy, S. X. Hu, D. N. Polsin, L. E. Crandall, M. F. Huff, D. A. Chin *et al.*, Phys. Rev. B **103**, 094115 (2021).

[27] G. Giuliani and G. Vignale, *Quantum Theory of the Electron Liquid* (Cambridge University Press, Cambridge, 2005).

[28] K. Matsuda, K. Tamura, M. Inui, Y. Kajihara, T. Nagao, M. Yao, M. Itou, and Y. Sakurai, Eur. Phys. J. Spec. Top. **196**, 95 (2011).

[29] W.-C. Pilgrim, D. Szubrin, F. Demmel, A. Orecchini, S. Rols, A. Laloni, and A. De Francesco, Europhys. Lett. **122**, 36005 (2018).

[30] V. F. Gantmakher, *Electrons and Disorder in Solids* (Oxford University Press, Oxford, 2005).

[31] L. D. Landau and E. M. Lifshitz, *Electrodynamics of Continuous Media* (Pergamon Press, Toronto, 1984).

[32] G. I. Kanel, A. S. Savinykh, G. V. Garkushin, and S. V. Razorenov, JETP Lett. **102**, 548 (2015).

[33] R. F. Trunin, L. F. Gudarenko, M. V. Zhernokletov, and G. V. Simakov, *Experimental Data on Shock Compression and Adiabatic Expansion of Condensed Matter* (RFNC-VNIIEF, Sarov, 2001).

[34] E. P. Pashuck and B. P. Pashaev, Teplofiz. Vys. Temp. **21**, 479 (1983) [in Russian].

[35] R. S. Hixson, M. A. Winkler, and J. W. Shaner, Physica B+C **139–140**, 893 (1986).

[36] L. D. Landau and E. M. Lifshitz, *Fluid Mechanics (Course of Theoretical Physics, Vol. 6)*, 2nd ed. (Pergamon Press, Oxford, 1987).

[37] W. M. Hodgson, Ph.D. thesis, Lawrence Livermore National Laboratory, Livermore, 1978.

[38] G. R. Gathers, Rep. Prog. Phys. **49**, 341 (1986).

[39] G. Pottlacher and H. Jäger, Int. J. Thermophys. **11**, 719 (1990).

[40] V. Ya. Ternovoi, V. E. Fortov, S. V. Kvitov, and D. N. Nikolaev, AIP Conf. Proc. **370**, 81 (1996).